DOI: 10.24352/UB.OVGU-2019-015 TECHNISCHE MECHANIK, 39, 1, (2019), 162 – 174
submitted: July 6, 2018

One-Dimensional Turbulence Simulations for Reactive Flows in Open and Closed Systems

T. Starick, J. A. Medina M., H. Schmidt

The One-Dimensional Turbulence (ODT) model is applied to reactive flows in open and closed systems represented by a lifted jet flame in a vitiated coflow, and a constant volume autoignition configuration, respectively. ODT is a one-dimensional model for turbulent flow simulations, which uses a stochastic formulation to represent the effects of turbulent advection. Diffusion and reaction effects along the ODT domain are considered by deterministic evolution equations.
This work is an effort to verify the applicability and efficiency of the model for open and closed systems. In the open system case, ODT results are compared against experimental results of a lifted methane/air jet flame detailed in the work of Cabra et al. (2005). In the closed system case, a periodic, constant volume domain is used to investigate the sensitivity of the ignition evolution to initial temperature and composition inhomogeneities of a lean n-heptane/air mixture. In the latter context, ODT results are compared to DNS results from Luong et al. (2015). The results for the jet and constant volume configuration show a reasonable match with the experimental and DNS data, considering the reduced order of the model and the underlying assumptions for each case. At the jet configuration, a dependence of the flame evolution on the turbulence intensity parameter can be seen. For the closed system, initial temperature and composition inhomogeneities allow a mitigation of the undesirable rapid pressure rise due to locally different ignition delay times.

1 Introduction

The topic of low temperature homogeneous premixed combustion has led to the development and optimisation of Homogeneous Charge Compression Ignition (HCCI) engines. These combine the benefits of spark and compression ignition engines. They are, however, confronted with the problem of simultaneous reaction of homogeneous mixture zones entailing a rapid pressure rise, which results in pressure ringing, engine knocking, or even the destruction of the engine block. Stratification is, therefore, an aspect that needs to be considered in the design to avoid a rapid pressure rise (Luong et al., 2015). Computationally, this has been studied by means of the effects of disturbances or inhomogeneities in reactive mixtures and temperature distributions by Yoo et al. (2011) and Luong et al. (2015).

The topic of flame extinction and flame stabilisation has also central importance, and it has been traditionally addressed experimentally and theoretically by the study of simplified jet flames. Lifted jet flames are a special category of jet flames, where the stabilised flame is lifted from the burner by increasing the fuel or air coflow velocity (Lyons, 2007). These flames may allow, e.g., the minimisation of the damage provoked by the flame to the burner construction materials. Past studies of Cabra et al. (2005) have confirmed autoignition as a mechanism for flame stabilisation in lifted flames.

There are clear limitations for fully accurate computational investigations of these phenomena. The most reliable approaches, Direct Numerical Simulations (DNS), are prohibitively expensive, since they require the complete resolution of all scales of interactions between turbulence and chemistry (Yoo et al., 2011; Yu and Bai, 2013; Luong et al., 2015). In contrast, 1-D models are still attractive for research due to the broad physical insight that they might offer at the expense of their relatively cheap computational cost. In an effort to resolve all relevant scales, yet still be able to achieve realistic Reynolds number flows in numerical simulations, Alan Kerstein formulated the One-Dimensional Turbulence (ODT) model (Kerstein, 1999). ODT is an efficient alternative in comparison to DNS, and an alternative in comparison to Reynolds-Averaged Navier-Stokes (RANS) and Large-Eddy Simulation (LES)

approaches, as demonstrated by several investigations done so far by Kerstein et al. (2001); Ashurst and Kerstein (2005); Lignell et al. (2013); Jozefik et al. (2015); Fragner and Schmidt (2017) and Medina M. et al. (2018).

In this study, a broad, yet brief overview of the ODT modelling framework for open and closed combustion systems is presented. Lignell et al. (2013) presented a comprehensive overview of all possible applications of ODT. The latter study, however, missed the topic of constant volume modelling completely. Initially homogeneous, yet disturbed, temperature and composition fields are evaluated with a recent ODT formulation in a constant volume, periodic configuration (Medina M. et al., 2018). Results for a lifted jet flame in a vitiated coflow, following a more traditional ODT formulation are shown as well (Echekki et al., 2001; Lignell et al., 2013).

2 ODT Model Formulation

2.1 Turbulent Advection and Eddy Event Implementation in ODT

The characteristic signature from ODT is the triplet map transformation (Kerstein, 1999). The implementation of a triplet map (eddy event) is a representation of the turbulent advection effects in an incompressible flow. This is a mere kinematic representation of the flow, and thus the analysis of the effects of a triplet map should be discussed within the framework of the momentum equation in an incompressible regime (divergence-free velocity field given by u_j, for $j = 1, 2, 3$). Starting from the momentum equation, it is possible to decompose the advection term into linear and non-linear contributions. The pressure can also be considered as a scalar field resulting from the sum of linear and non-linear contributions. Considering only linear effects, the momentum equation for incompressible flows in ODT, assuming the 1-D line direction as y, results in,

$$\frac{\partial u_j}{\partial t} = \nu \frac{\partial^2 u_j}{\partial y^2} + E_j + \Gamma. \tag{1}$$

A source term Γ has been added to the original ODT momentum equation as described in Kerstein et al. (2001). This symbolises the linear effects of mean advection or a mean forcing pressure gradient. This convention was chosen to represent the source term treatment in ODT (Lignell et al., 2013; Fragner and Schmidt, 2017). In Eq. (1), t is the time, $\nu = \mu/\rho$ is the kinematic viscosity (μ is the dynamic viscosity and ρ the density) and E_j represent changes induced by the triplet map and pressure scrambling operations in ODT detailed in the work of Kerstein et al. (2001).

In general, the triplet map implementation causes a change in a scalar profile along the line direction, according to the transformation rule,

$$\psi(y) \rightarrow \psi[f(y)]. \tag{2}$$

Here, ψ is any scalar quantity defined in the ODT line at a position y and subsequently mapped to a position $f(y)$ by the transformation rule (Kerstein, 1999). The transformation rule is measure preserving, which for constant density and a scalar velocity component implies conservation of $\int u^0 \mathrm{d}y$, $\int u^1 \mathrm{d}y$, $\int u^2 \mathrm{d}y$; i.e., the transformation implies conservation of mass (length), momentum and energy along the line. Treating the velocity as a vector requires the use of a Kernel function, which redistributes the available kinetic energy among velocity components (Kerstein et al., 2001). Since it is clear that for this work, the previous conception of ODT with constant density is rather limited, the expansion for the variable density formulation, introduced by Ashurst and Kerstein (2005), is used for the mapping of the velocity field u_j, namely

$$u_j(y) \rightarrow u_j[f(y)] + b_j K(y) + c_j J(y). \tag{3}$$

Here, $K(y)$ and $J(y)$ are kernel functions, as described in Ashurst and Kerstein (2005), while b_j and c_j are the respective kernel coefficients for each velocity component. The reader should note that, although the introduction of two kernels for the velocity mapping in Eq. (3) allows redistribution of available kinetic energy in a variable density line, the fundamental conception of the map as a measure preserving transformation is more readily applicable for solenoidal flows (Lignell et al., 2013) (and in fact, it is formulated by Ashurst and Kerstein (2005) for flows with negligible compressibility effects). It is therefore convenient to introduce a splitting of the velocity field into its solenoidal and irrotational components. The solenoidal component (rotational part) is readily handled by the eddy event conception in ODT, while the irrotational component $u_{tot,j}$ can be decomposed into a deformation component $u_{D,j\,\text{(deformation)}}$ and a linear advection component $u_{A,j,\,\text{(net advection)}}$ as described in Medina M. et al. (2018).

$$u_{tot,j} = u_{A,j\,\text{(net advection)}} + u_{D,j\,\text{(deformation)}} \tag{4}$$

The net advection of u_j in Eq. (4) refers to the sum of mean and turbulent advection. This is the starting point for the formulation of the set of governing equations in the applicable ODT model. u_j is governed by a quasi-incompressible momentum evolution, while $u_{D,j}$ arises exclusively from the variable-density (compression and expansion) effects along the line ($u_{D,2} = u_D$ and $u_{D,1} = u_{D,3} = 0$) (Medina M. et al., 2018).

In ODT, eddy events are sampled from a joint Probability Density Function (PDF) $P(l, y_0, t)$ of eddy sizes l and positions y_0 at a given time t (Kerstein, 1999). The reconstruction of the PDF at every instant of time is prohibitively expensive, since it requires evaluating all possible potential eddies with any size l at any position y_0. A discrete approximation of the PDF is used instead, constructed by a combination of the rejection method and the thinning method (Kerstein, 1999). The sampling conforms then with a defined, statistical Poisson process. Generally speaking, an acceptance probability of the eddy $P_a(l, y_0, t)$ is obtained by the expression,

$$\frac{\lambda(l, y_0, t)}{f(l)g(y_0)} \Delta t_{sampling} = P_a(l, y_0, t). \tag{5}$$

Eq. (5) is able to correctly approximate the eddy sampling from $P(l, y_0, t)$, as long as the sampling time interval $\Delta t_{sampling}$ is sufficiently small ($\Delta t_{sampling} << 1$). $\lambda(l, y_0, t)$ is an eddy rate in ODT, while $f(l)$ and $g(y_0)$ are assumed PDFs for the eddy size and position, as in Lignell et al. (2013). $\lambda(l, y_0, t)$ can be modelled based on a dimensional analysis relating energetic contributions to the inverse of an eddy turnover time τ, as in Jozefik et al. (2015) and Medina M. et al. (2018),

$$\lambda(l, y_0, t) = \frac{C}{l^2 \tau} = \frac{C}{l^2} \left[\frac{2K_0}{\rho_0} \left(E_{kin} - Z E_{vp} + E_{pe} \right) \right]^{1/2}. \tag{6}$$

Eq. (6) models the eddy turnover time in ODT in terms of the available (kinetic) energy E_{kin}, an energetic viscous penalty E_{vp}, and a potential energy term E_{pe}. The latter is added in order to influence the eddy selection due to the variable density line (Jozefik et al., 2015; Medina M. et al., 2018). C and Z are model parameters, which are normally calibrated for a specific flow configuration. The terms $K_0 = l^{-3}(\int_{y_0}^{y_0+l} K^2 \mathrm{d}y)$ and $\rho_0 = \int_{y_0}^{y_0+l} \rho K^2 \mathrm{d}y$, are used with the definitions of the different energies,

$$E_{kin} - Z E_{vp} + E_{pe} = \left[K_0 \left(Q_1 + Q_2 + Q_3 \right) \right] - Z \left[\frac{1}{2} \left(\frac{\mu_{eddy}^2}{\rho_{eddy} l} \right) \right] + \left[K_0 \int_{y_0}^{y_0+l} \frac{\partial u_D}{\partial t} K \left(\rho - \rho_{eddy} \right) \mathrm{d}y \right]. \tag{7}$$

Here, Q_1, Q_2 and Q_3 are the available energies per velocity component, as in Ashurst and Kerstein (2005). μ_{eddy} and ρ_{eddy} are line averages of the dynamic viscosity and density (averages over the eddy length).

After an eddy is implemented, a deterministic catch up takes place up to the physical time at which the eddy was deemed to be implemented. This is the instant of time t at which the eddy was accepted according to the sampling based on $P_a(l, y_0, t)$. The deterministic catch up mechanism consists of a time-advancement of the 1-D diffusion/reaction evolution equations in ODT, starting at the instant of time corresponding to the last eddy implementation, up to the time t. Therefore, time advances constantly due to the increments $\Delta t_{sampling}$. The numerical solution as a whole advances effectively with every performed catch up. The deterministic 1-D diffusion/reaction evolution equations in ODT are detailed in the next section.

2.2 ODT Diffusion/Reaction Evolution for Closed Systems (Constant Volume Configuration)

This section gives an overview of the diffusion/reaction evolution equations for closed systems used in ODT. For a detailed description of the numerical advancement for the ODT diffusion/reaction evolution equations, the reader is referred to Appendix I.

The diffusion/reaction evolution equations in ODT can be derived from the application of the Reynolds Transport Theorem (RTT) to the intensive quantities (ϵ) of mass, momentum and energy. For reference, the Lagrangian formulation of the equations, using a zero Mach number limit approximation, is obtained and explained in Lignell et al. (2013). Here, the equations obtained from Lignell et al. (2013) are only mentioned and written in an equivalent differential form. Momentum conservation in the ODT line, considering that the cell interfaces move with the mass average velocity (no ϵ property fluxes across the cells), implies, for the quasi-incompressible treatment of the velocity u_j,

$$\rho \frac{\mathrm{d}u_j}{\mathrm{d}t} = \frac{\partial}{\partial y} \left(\mu \frac{\partial u_j}{\partial y} \right). \tag{8}$$

Here, $\mathrm{d}/\mathrm{d}t$ symbolises the Lagrangian time derivative. Similarly, diffusion and reaction evolution of species mass fractions Y_k ($k \in \{1, 2, ...N\}$), is given by,

$$\rho \frac{\mathrm{d}Y_k}{\mathrm{d}t} = \frac{\partial}{\partial y}\left(\rho D_k \frac{\partial Y_k}{\partial y} + \frac{\rho D_k Y_k}{M}\frac{\partial M}{\partial y}\right) + \dot{w}_k. \tag{9}$$

In Eq. (9), D_k is the kth species mixture-averaged diffusion coefficient, M is the mean molecular weight of the mixture and $\dot{w}_k$ is the kth species reaction rate. The Hirschfelder and Curtis' approximation for the species diffusion velocities is considered here, i.e. $V_k = -D_k\left(Y_k^{-1}\partial Y_k/\partial y + M^{-1}\partial M/\partial y\right)$.

The evolution equation for the enthalpy of the mixture h is,

$$\rho \frac{\mathrm{d}h}{\mathrm{d}t} = \frac{\mathrm{d}P}{\mathrm{d}t} + \frac{\partial}{\partial y}\left(\lambda \frac{\partial T}{\partial y}\right) - \frac{\partial}{\partial y}\left[\sum_{k=1}^{N}\left(h_k \rho V_k Y_k\right)\right]. \tag{10}$$

In Eq. (10), P is the leading order thermodynamic pressure, λ is the thermal conductivity, T is the temperature of the mixture and h_k is the kth species specific enthalpy.

As in Medina M. et al. (2018), the divergence condition for the deformation velocity allows the calculation of the temporal rate of change of the thermodynamic pressure (applying an integration over the ODT line). It also allows the calculation of the dilatation of the cells, which is required to enforce mass conservation, once the new thermochemical state is known (local divergence of each cell).

$$\frac{\partial u_D}{\partial y} = -\frac{1}{\gamma P}\frac{\mathrm{d}P}{\mathrm{d}t} + \Psi. \tag{11}$$

In Eq. (11), γ is the ratio of specific heats and Ψ is defined as

$$\begin{aligned}\Psi = \frac{1}{\rho c_p T}\Bigg\{ & \frac{\partial}{\partial y}\left(\lambda \frac{\partial T}{\partial y}\right) - \frac{\partial}{\partial y}\left[\sum_{k=1}^{N}\left(h_k \rho V_k Y_k\right)\right] \\ & + \sum_{k=1}^{N}\left[h_k\left(\frac{\partial}{\partial y}\left(\rho V_k Y_k\right) - \dot{w}_k\right)\right]\Bigg\} \\ & - \frac{M}{\rho}\sum_{k=1}^{N}\left\{\frac{1}{M_k}\left[\frac{\partial}{\partial y}\left(\rho V_k Y_k\right) - \dot{w}_k\right]\right\},\end{aligned} \tag{12}$$

c_p is the specific heat capacity at constant pressure. The equations for species and enthalpy evolution are solved by means of a Strang-Splitting method (Medina M. et al., 2018). The $\mathrm{d}P/\mathrm{d}t$ term used in Eq. (10) is calculated from the integration of Eq. (11). The resulting pressure at the end of the advancement is calculated by a closed form of the ideal gas law,

$$P = \frac{R\left(\int_{y=0}^{y=L}\rho \mathrm{d}y\right)_{t=0}}{\int_{y=0}^{y=L}\left(T\sum_k \frac{Y_k}{M_k}\right)^{-1}\mathrm{d}y}. \tag{13}$$

Here, L is the length of the 1-D domain and R is the universal gas constant. The quantity in the numerator in Eq. (13) indicates the initial mass of the line, which remains constant during the simulation. After the pressure update, the density is calculated by means of the ideal gas law. Momentum is integrated with an implicit Euler method prior to the pressure and density update, but with the updated temperature derived from the advancement of h and Y_k. Finally, cell sizes are adjusted to enforce mass conservation, based on the use of the definition $u_D = \mathrm{d}y/\mathrm{d}t$ in the local divergence constraint, Eq. (11) (evaluated at the new thermochemical state) (Medina M. et al., 2018).

2.3 ODT Diffusion/Reaction Evolution for Open Systems (Jet Configuration)

The diffusion/reaction equations for the open system configuration are in general the same ones as those derived for the closed system. For open systems, we have $\mathrm{d}P/\mathrm{d}t = 0$ in Eq. (10) and (11). Eq. (13) is also redundant, since the pressure stays constant.

The divergence condition is enforced in the open configuration in a slightly different way. It is possible to rewrite Eq. (11) as

$$\frac{\partial u_D}{\partial y} = -\frac{1}{\rho}\frac{\mathrm{d}\rho}{\mathrm{d}t}. \tag{14}$$

Within the Lagrangian framework of the model, it is possible to approximate numerically $\mathrm{d}\rho/\mathrm{d}t$. Using a Leapfrog time approximation and applying the definition of velocity $u_D = \mathrm{d}y/\mathrm{d}t$, while considering the midpoint time-levels as the averages of time-levels n and $n+1$, mass conservation is obtained as in Lignell et al. (2013),

$$(\rho\Delta y)^{n+1} = (\rho\Delta y)^{n}\,. \tag{15}$$

Eq. (15) corresponds to the integral conservation of mass within a cell. It dictates the corresponding adjustment of the cell sizes that conforms with mass conservation in an open system. Unlike Eq. (11) for closed systems, using Eq. (15) may result in changes of the overall 1-D domain length.

In this work, a comparison with stationary spatially developing round jet flames is intended. Following Echekki et al. (2001), the 1-D domain is advected in z-direction using an instantaneous bulk velocity $\overline{u}(t)$,

$$z(t) = z(t_0) + \int_{t_0}^{t} \overline{u}(t')\mathrm{d}t'. \tag{16}$$

The bulk velocity in Eq. (16) is calculated by the sum of the free-stream (coflow) velocity u_∞ and the ratio of the integrated momentum flux to the integrated mass flux,

$$\overline{u}(t) = u_\infty + \left.\frac{\int_{-\infty}^{\infty}\rho\left(u-u_\infty\right)^2\mathrm{d}y}{\int_{-\infty}^{\infty}\rho\left(u-u_\infty\right)\mathrm{d}y}\right|_t. \tag{17}$$

Unlike in the closed configuration, the open configuration is solved by means of a first-order explicit Euler advancement, as in Lignell et al. (2013).

3 Results

3.1 Closed System (Constant Volume Configuration)

Simulations for constant volume autoignition of a lean n-heptane/air mixture were performed with ODT using the same settings as in the DNS from Luong et al. (2015). The domain extends over 3.2 mm. Periodic boundary conditions are applied on the ODT line. The initial grid is discretised by a uniform distribution of 1280 cells along the line. Randomised initial fields for the velocity and scalars were generated based on a Passot-Pouquet spectrum (Passot and Pouquet, 1987) that conforms with a given mean and RMS fluctuation value, as in Oevermann et al. (2008) and Medina M. et al. (2018). The same version of the ODT code as in Medina M. et al. (2018) was used for the simulations and applies an adaptive solver that enables local temporal changes in the resolution, in order to accurately capture all scales along the ODT line (Lignell et al., 2013).

Table 1 lists the settings for mean initial temperature and equivalence ratio, T_0 and ϕ_0, and fluctuations of temperature T', equivalence ratio ϕ' and velocity u' for the investigated cases. The most energetic length scales for

Table 1: Parameters of the simulation cases 1-4, considering either temperature T or composition Φ inhomogeneities.

Case	T_0	T'	ϕ_0	ϕ'	l_e, l_{Te}, l_{ϕ_e}	u'	${\tau_{ig}}^0$
	(K)	(K)	(-)	(-)	(mm)	(m/s)	(ms)
1	805	15	0.45	-	1.25	0.83	1.5
2	933	15	0.45	-	1.25	0.83	1.5
3	805	-	0.45	0.05	1.25	0.83	1.5
4	933	-	0.45	0.05	1.25	0.83	1.5

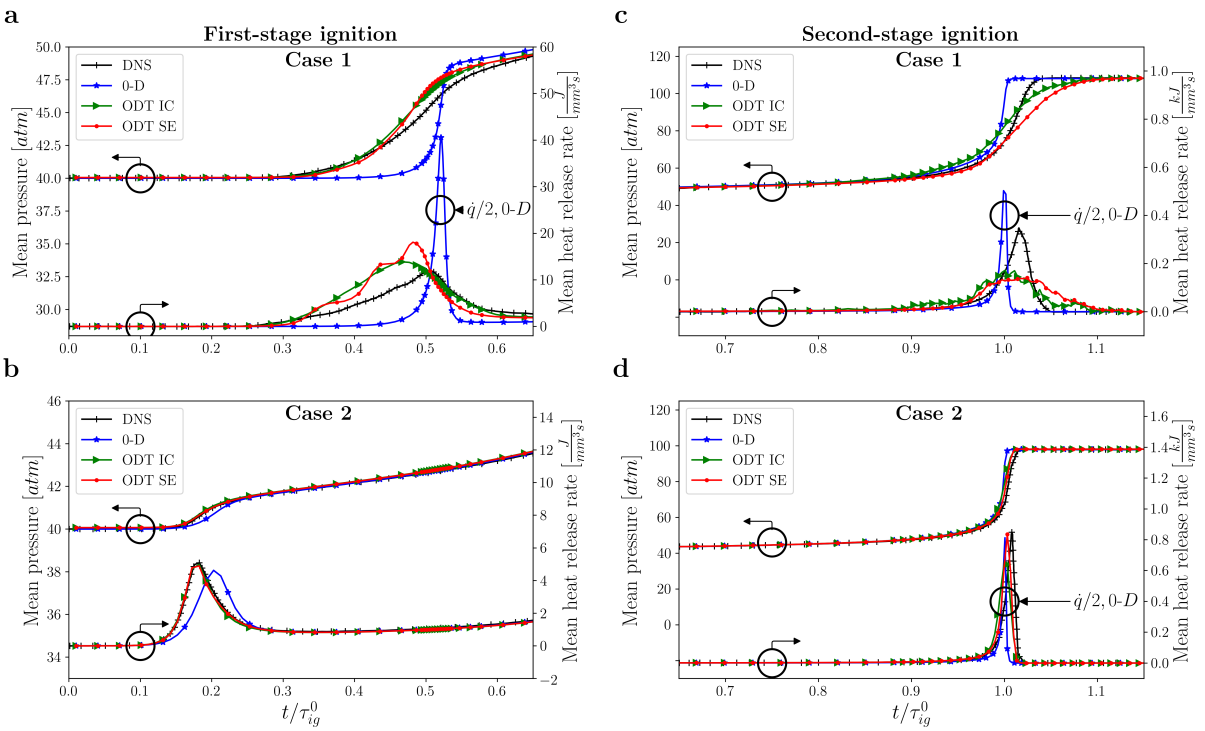

Figure 1: Temporal evolution of the spatially averaged pressure and heat release rate for case 1 and 2. These consider temperature inhomogeneities of $\boldsymbol{T' = 15}$ K at initial mean temperatures of $\boldsymbol{T_0 = 805}$ K (a and c) and $\boldsymbol{T_0 = 933}$ K (b and d).

temperature l_{Te}, composition $l_{\phi e}$ and velocity l_e are also presented, as well as the 0-D ignition delay time τ_{ig}^0, taken from Luong et al. (2015). The integral length scales are assumed to be equal to the most energetic length scales for the generation of the initial conditions. The initial pressure in the domain is $P_0 = 40$ atm, as in the DNS.

The chemistry for the n-heptane/air combustion is represented by a 58-species reduced kinematic mechanism from Yoo et al. (2011), as in the DNS. For the calculation of the thermodynamic and transport properties, the C++ interface of the Cantera software package is applied (Goodwin, 2002). During the reaction step of the splitting, the stiff chemistry is solved by means of CVODE (Hindmarsh and Serban, 2015) (the reaction component of the enthalpy is advanced simultaneously with an explicit Euler method).

ODT model parameters C and Z in Eq. (6) are taken as $C = 4$ and $Z = 0.4$. For this specific case, C represents the intensity of the turbulence in ODT, while Z is a proportionality parameter of order one for the energetic viscous penalty, as in Kerstein et al. (2001). These values were selected based on a calibration process of the model for one of the cases studied, and assumed constant for all simulations.

The initial mean temperature values of $T_0 = 805$ K and $T_0 = 933$ K were deliberately selected. The characteristic combustion behaviour of n-heptane/air mixtures with an equivalence ratio of $\phi_0 = 0.45$ leads to the same ignition delay time of $\tau_{ig}^0 = 1.5$ ms for $T_0 = 805$ K and $T_0 = 933$ K in the 0-D simulation (Luong et al., 2015).

Figure 1 shows the temporal evolution of the spatial and ensemble averaged ODT results for heat release rate and pressure. Results are shown for the first-stage ignition (left) and second-stage ignition (right). For comparison, 0-D and DNS data from Luong et al. (2015) are shown as well. The 0-D results served as a validation of the ODT code, since they were obtained by a homogeneous initialisation of the 1-D fields and by suppressing all possible eddy events. For a better visualisation, the 0-D values are sometimes shown with a normalisation factor of 0.5.

The distribution of the initial temperature and composition fields has a large influence on the combustion process and thus on the ignition delay time. This can be seen in Fig. 1, which considers random initialisations (ODT IC in the plots) and a sample size of $n = 100$ for every case detailed in Table 1.

Due to the stochastic nature of the ODT model, an evaluation of the influence of initial conditions and of the stochastic turbulent transport implementation was performed separately. In this context, an initial condition was

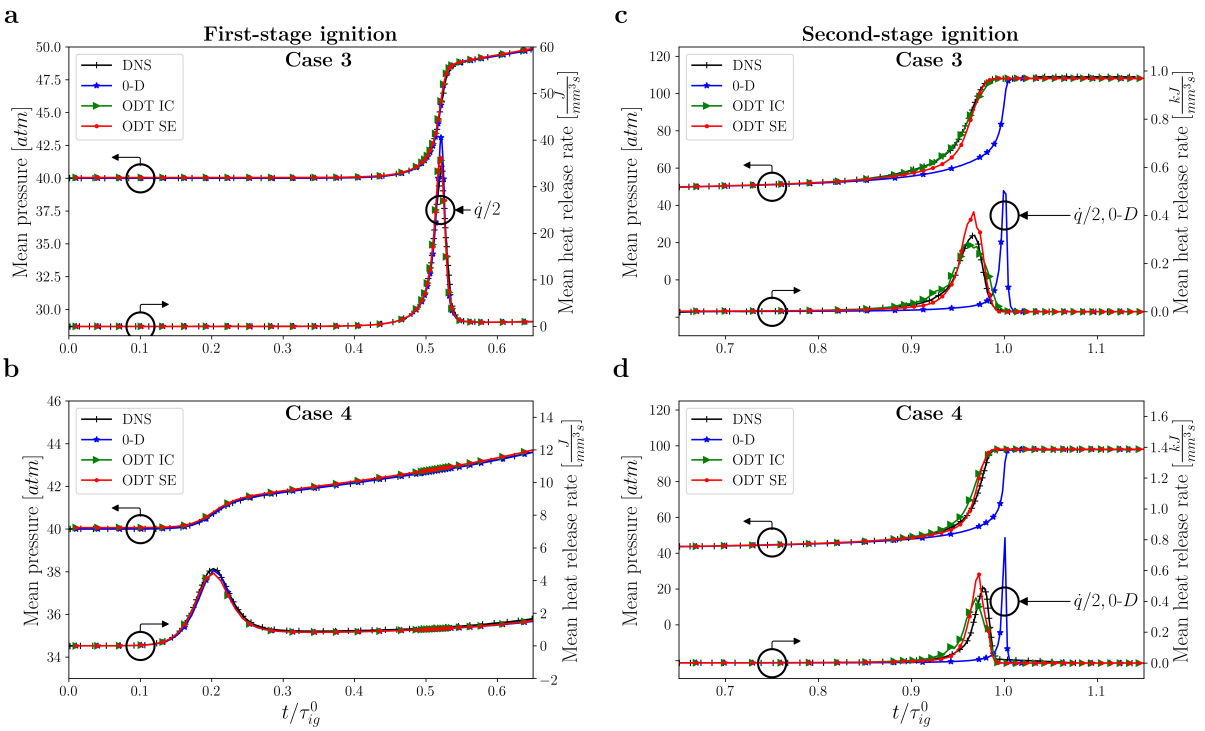

Figure 2: Temporal evolution of the spatially averaged pressure and heat release rate for case 3 and 4. These consider composition inhomogeneities of $\boldsymbol{\Phi' = 0.05}$ at initial mean temperatures of $\boldsymbol{T_0 = 805}$ K (a and c) and $\boldsymbol{T_0 = 933}$ K (b and d).

selected, which best suited the DNS data in temporal development of pressure and spatially averaged heat release rate. Several simulations were then performed and ensemble averaged. Despite the same initial conditions, the simulation results are still subject to fluctuations due to the stochastic eddy event implementation. This can also be seen in Fig. 1 (ODT SE in the plots).

In general, ODT is able to reproduce results that match the DNS data at the first and second-stage ignition. 0-D results from Luong et al. (2015) show that slight modifications in the initial mean temperature of $T_0 = 805$ K have a greater influence, in comparison to $T_0 = 933$ K, on the ignition delay time. This can be one possible reason for the wider spread of the dome of heat release rate and the less steep pressure rise of the ensemble averaged ODT results at case 1 (ODT IC, ODT SE) when comparing with DNS data. The temperature fluctuations cause a delay in combustion, whereby the pressure rise is mitigated. In case 2, initial temperature fluctuations have less influence on the combustion process. For the latter case, 0-D, ODT IC, ODT SE and DNS results have similar profiles.

Figure 2 also shows the temporal evolution of the spatially and ensemble averaged ODT results for heat release rate and pressure during first-stage ignition (left) and second-stage ignition (right). In contrast to Fig. 1, however, composition inhomogeneities of $\phi' = 0.05$ are examined. Again, ODT (ODT IC and SE) is able to produce results that are in very good agreement with the DNS trend. This applies to both the first-stage ignition and the second-stage ignition. ODT SE slightly overpredicts and ODT IC slightly underpredicts the DNS results at the moment of combustion in cases 3 and 4. The comparison with the 0-D simulations shows that the composition fluctuations lead to an earlier combustion for both investigated initial mean temperatures. The rapid pressure rise is only slightly mitigated by the composition fluctuations.

Overall, results obtained with ODT show a reasonable match with DNS data. The quality of the results is promising, considering the short simulation times and the reduced dimensionality application of this ODT model for constant volume combustion.

3.2 Open System (Jet Configuration)

The open system case is represented by a lifted methane/air jet flame in a vitiated hydrogen/air coflow. For comparison purposes, ODT simulations consider an equivalent setup and the same parameters as the experimental measurements of Cabra et al. (2005). Table 2 lists the initial conditions for the jet and coflow. Here, Re is the bulk Reynolds number based on d, the diameter, u is the velocity, T is the temperature and X the mole fraction of each species. For the initial velocity profile at the nozzle exit, a synthetic profile was used which was created by superposition of a fully developed turbulent channel flow mean profile with a turbulent Passot-Pouquet spectrum (Passot and Pouquet, 1987). The coflow was initialised with a uniform radial distribution of the velocity at $z/d = 0$ (nozzle exit), where z stands for downstream position (Eq. (16)) and d for the diameter of the jet.

Table 2: Initial conditions for the jet and coflow are listed.

-	Jet	Coflow
Re	$28,000$	$23,300$
d(mm)	4.57	140
u(m/s)	100	5.4
T(K)	320	1350
X_{O_2}	0.15	0.12
X_{N_2}	0.52	0.73
X_{H_2O}	0.0029	0.15
X_{OH}(ppm)	0.0	200
X_{H_2}(ppm)	100	100
X_{CH_4}	0.33	0.0003

The ODT domain uses homogeneous Neumann boundary conditions and has a length of 140 mm, which is a span close to 30 jet diameters. Although the ODT formulation for open systems using a planar and temporal framework is not novel, the chosen configuration represents nonetheless a challenge for the model, given the delicate interactions and balance between the mixing of the hot coflow products and the cold unburned jet, together with the reaction and autoignition of the jet (Cabra et al., 2005).

For the representation of the methane/air chemistry, a 19-species reduced mechanism from Lu and Law (2008) is used. This mechanism is derived from a 30-species skeletal mechanism for methane/air based on the detailed GRIMech 3.0 mechanism (Smith et al., 1999).

Figure 3, on the left side, shows a two-dimensional rendering of the temperature evolution of the jet flame for one realisation. On the right side, an ensemble averaged temperature evolution of the jet flame is presented with a sample size of $n = 50$. Axis y/d corresponds to the one-dimensional domain, while axis z/d is obtained by means of the temporal-to-spatial translation, Eq.(16). The ODT model parameters were fixed to $C = 5$ and $Z = 50$. The ensemble averaged temperature evolution on the right side shows the familiar structure of a jet diffusion flame. This supports the validity of the assumption that the streamwise velocity associated with the chemically active region can be approximated by a bulk velocity, which is advecting the 1D-domain in downstream direction. The visually determined liftoff height of $z/d \approx 38$ in Figure 3 is in good agreement with the findings of Cabra et al. (2005).

In Figure 4, the concentration evolution of the OH-species is presented for a single realisation on the left side and an ensemble average on the right side. The comparison of the ensemble averaged temperature evolution in Figure 3 and OH-concentration evolution in Figure 4 shows that the highest OH-concentrations occur in the regions with the highest temperatures.

Figure 5 presents the Favre-averaged centerline profile of temperature and O_2 mass fraction for different values of the C model parameter. The averaging is based on 50 ensemble members for every case simulated with randomised initial profiles. A detailed previous study of the application of ODT for jet flames has been performed recently by Abdelsamie et al. (2017). Abdelsamie et al. showed that the model parameter C has a large influence on ignition prediction and scalar conditional means when comparing ODT results against DNS data.

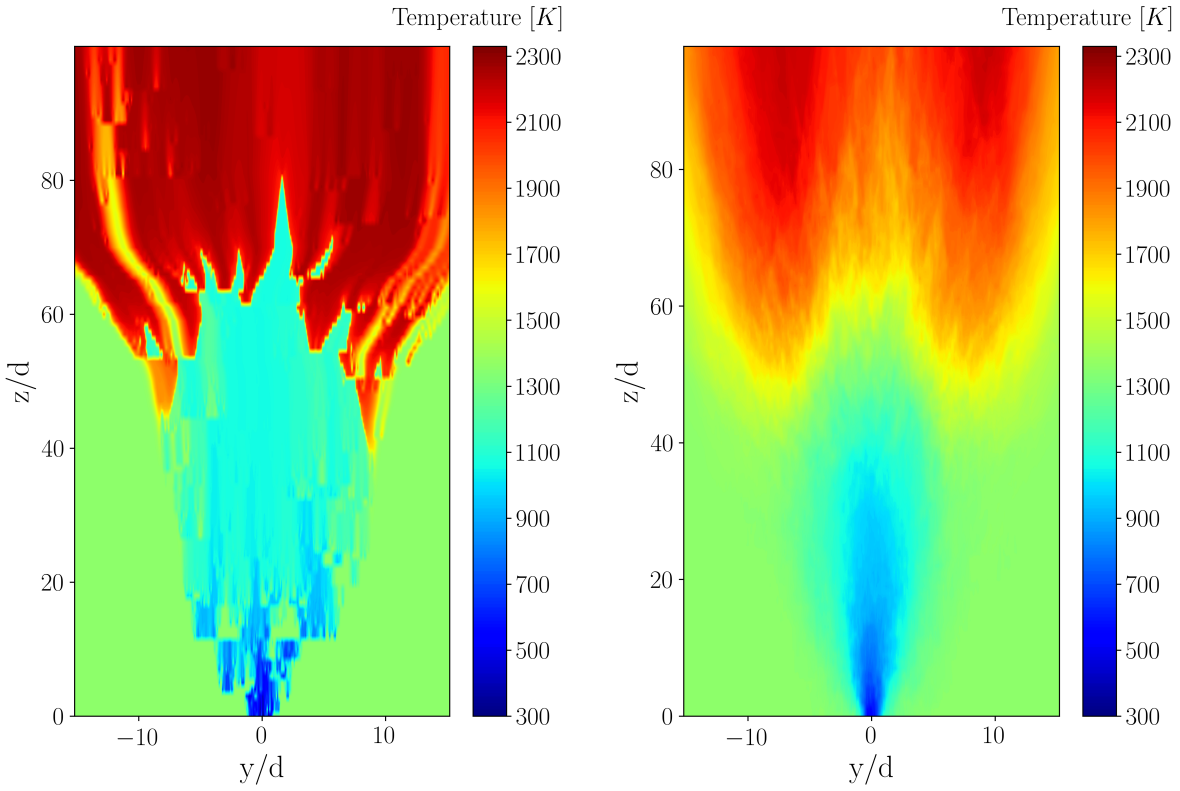

Figure 3: Two-dimensional rendering of temperature evolution for a single realisation (left) and ensemble average (right).

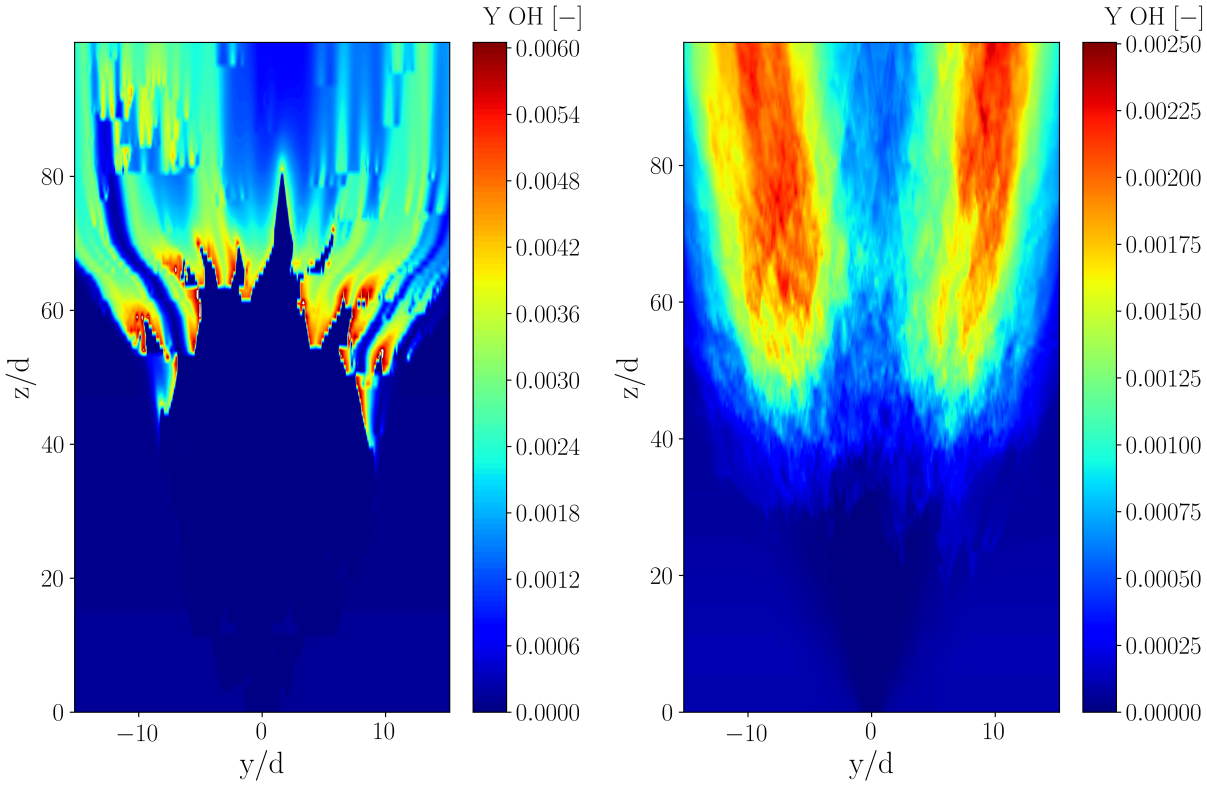

Figure 4: Two-dimensional rendering of OH-concentration evolution for a single realisation (left) and ensemble average (right).

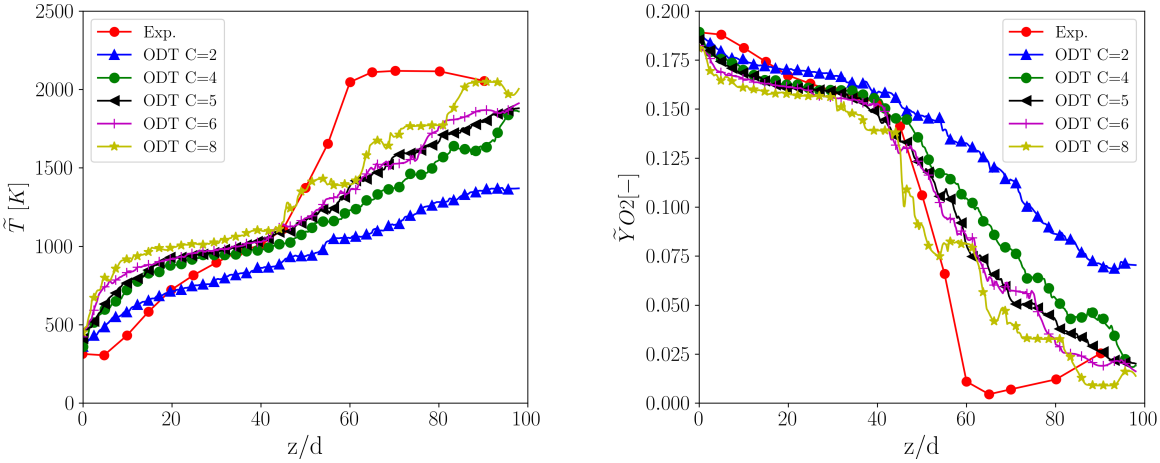

Figure 5: Comparison of simulated centerline profiles of Favre-averaged temperature (left) and Favre-averaged O_2 mass fraction (right) against experimental results (Exp.) of Cabra et al. (2005). For the ODT simulations, the model parameter C was varied.

Results shown in Figure 5 confirm the findings of Abdelsamie et al. (2017) for the C parameter. The initial stage (up to $z/d \approx 25$) characterised by mixing without reaction between jet and coflow is strongly affected by the C parameter. A high C parameter encourages the mixing and leads to a fast temperature increase at the centerline. This tends to accelerate the ignition. However, higher C parameters exaggerate the mixing in igniting zones and lead to a suppression of the ignition. In contrast, lower C parameters underestimate the mixing. The consequence of this is an insufficient mixing of the cold jet and hot coflow that results in a later ignition. A moderate C parameter of $C = 5$ and $Z = 50$ gave the best compromise for this study.

4 Conclusions

The application of ODT for simulations of a constant volume configuration and a jet is presented. The constant volume configuration is aimed at evaluating autoignition of a n-heptane/air mixture with initial temperature and composition inhomogeneities. The predicted heat release rates and pressure rises for all investigated cases are found to be in reasonable agreement with the DNS results, considering the reduced order of the model. The model is able to capture the key combustion characteristics of the examined n-heptane/air autoignition processes.

Despite the required number of ensemble members, which can be calculated in parallel following a Monte Carlo philosophy, simulation times for one ensemble member were in the order of 24 CPU-hours. These short computing times, in general, are one of the most attractive aspects of ODT. Although it is not done in detail in this work, parametric studies for different turbulent Reynolds number regimes and sensitivity analysis for reaction chemistry can be carried out with ODT, given the advantage of these short computing times. These investigations are currently not feasible with DNS due to the limitations in computing power (or only possible with great sacrifices in the reduction of chemical mechanisms). This makes ODT an efficient stand-alone model for constant volume configurations of reactive flows.

The second application of ODT is a lifted methane/air jet flame in a vitiated coflow. The spatially developing round jet flame is approximated by a planar temporally evolving jet. This assumption is not completely accurate and can be investigated in future work with a novel cylindrical ODT formulation from Lignell et al. (2018). Nonetheless, a good agreement was obtained in terms of centerline temperature evolution. The jet flame results reveal a strong influence of the C model parameter. The C parameter influences the mixing at the initial stage, which largely effects the entire combustion behaviour.

I Appendix

Numerical procedure for the constant volume configuration

In this appendix, we present additional details regarding the numerical advancement of the ODT equations already presented in Section 2. Both numerical methods used for the open and closed system have been previously explained in Lignell et al. (2013) and Medina M. et al. (2018). There are, however, some subtleties regarding the closed system implementation that may interest the reader. The reader is advised that the entire discussion in this appendix is focused on the numerical advancement of the ODT diffusion/reaction evolution equations presented in Section 2.2. The handling of the turbulent advection and eddy event implementation in Section 2.1 is out of the discussion, since the same strategy as in any previous ODT publication is applied.

Lignell et al. (2013) presented a Lagrangian ODT implementation using a Finite Volume Method (FVM) for combustion systems. Although this implementation is very appealing and fully conservative, it encounters theoretical obstacles for its application to closed systems. Especially, the compromise to displace the discrete volume interfaces in order to account for conservation of mass in the Lagrangian framework is challenging. This treatment conspires directly with the suppositions of a closed system with a fixed and constant volume. As noted in Lignell et al. (2013), a first order approximation of the continuity equation is,

$$\int_{\widehat{\Omega}} \rho \mathrm{d}V = 0 \rightarrow \rho_i \Delta y_i = Ci. \tag{18}$$

Here, $\widehat{\Omega}$ is a moving Lagrangian Control Volume (CV), ρ is the local density and Ci is a cell-wise constant. The volume elements in the 1-D domain are symbolised by the size of the discrete cells Δy_i. Eq. (18) allows the dilatation or contraction of the volume elements, and thus, of the overall Lagrangian system, in order to ensure conservation of mass. This equation conserves the mass of each cell, however, changes the volume of the cells. Summing up all volume elements results in a net volume change. This is done for open systems. This could also be applicable in closed systems with fixed volume, where mass and volume can both be conserved if a mean constant density is achieved. In such case, the calculation of the pressure that would satisfy Eq. (18) would be, in the opinion of the authors, iterative in its essence. Since the main purpose of ODT as a turbulence model is to facilitate access to turbulence states which cannot be reached by DNS, we opt to discard an iterative method for the advancement of the governing equations, and therefore choose a non-conservative formulation for the deterministic catch up of eddies in ODT. We explain this implementation in terms of Finite Difference (FD) equations, which are, in 1-D, conveniently equivalent to the discrete FVM representation.

Let us start the discussion defining the total time derivative for intensive quantities (ψ) in a Lagrangian system, $\mathrm{d}\psi/\mathrm{d}t = (\partial\psi/\partial t) + u_{tot,j}(\partial\psi/\partial x_j)$. Such a derivative is viewed in an Eulerian framework in terms of the partial rate of change and the advection of ψ. As discussed in Section 2.1, we can formally split the velocity $u_{tot,j}$ into its advective and dilatational part, in analogy to a Helmholtz decomposition. Neglecting the mean advection of the system, and considering turbulent advection only by the instantaneous eddy events in ODT, it is clear that the only effects that need to be incorporated in the total time derivative, besides the local Eulerian rate of change of ψ, are the dilatation effects by $u_{D,j} = u_D$. Due to our 1-D treatment, these dilatation effects are entirely given by the velocity divergence condition in Eq. (11). We can now relate the velocity divergence condition, and the velocity itself, to the Lagrangian interface displacement,

$$u_D = \frac{\mathrm{d}y}{\mathrm{d}t}. \tag{19}$$

Therefore, we can rewrite the divergence condition using a Central Difference Scheme (CDS) as,

$$\frac{\left.\frac{\mathrm{d}y}{\mathrm{d}t}\right|_{i+1/2} - \left.\frac{\mathrm{d}y}{\mathrm{d}t}\right|_{i-1/2}}{\Delta y_i} = -\frac{1}{\gamma_i P}\frac{\mathrm{d}P}{\mathrm{d}t} + \Psi_i. \tag{20}$$

In order to formulate a consistent discretisation, both Left-Hand Side (LHS) and Right-Hand Side (RHS) must be frozen at the same time level. The RHS of Eq. (20) is that one of Eq. (11) and includes the time-derivative of the pressure $\mathrm{d}P/\mathrm{d}t$, which must also be calculated at the corresponding time level. Below, we list the algorithmic solution steps of the ODT equations for the closed system configuration.

1. Start with some initial conditions for the density ρ, pressure P, enthalpy h, composition Y_k and ODT velocities u_j.

2. Calculate the corresponding $\mathrm{d}P/\mathrm{d}t$ at the fixed volume initial state (integrating Eq. (11) in Section 2.2),

$$\frac{\mathrm{d}P}{\mathrm{d}t} = -\left[(u_{D,y=L} - u_{D,y=0}) - \int_{y=0}^{y=L} \Psi_i \mathrm{d}y\right] \frac{P}{\int_{y=0}^{y=L} \frac{1}{\gamma}\mathrm{d}y}. \tag{21}$$

3. Advance the local Eulerian rate of change for the chemistry (h, Y_k) and the kinematics (u_j). In this work, a Strang-Splitting method for the diffusion and reaction operators is used as in Medina M. et al. (2018). This is done in order to tackle stiff chemistry problems. In principle, a forward Euler time integration would also be possible.

4. Calculate the resulting pressure at the new thermochemical state. As suggested by Motheau and Abraham (2016), we use an integral expression for the pressure, which is derived from mass conservation and the condition of constant mean density in the system (Eq. (13) in Section 2.2). This is still a resulting pressure in an Eulerian reference frame, thus, the discrete cell volumes are still frozen at this point.

5. Calculate the resulting local density using the new pressure, by means of the ideal gas law.

6. Determine the displacement of the Lagrangian cell interfaces by Eq. (20). Note that $\mathrm{d}P/\mathrm{d}t$ must be recalculated here. In this case, by using a first-order approximation in time, the resulting cell volumes are given as

$$\Delta {y_i}^{n+1} = \Delta {y_i}^{n} + \Delta t \left[\Delta y^* \left(-\frac{1}{\gamma_i^* P^*}\frac{\mathrm{d}P^*}{\mathrm{d}t} + \Psi_i^*\right)\right]. \tag{22}$$

7. The last step conforms with a first-order Lie-Splitting treatment for the Lagrangian total time derivative; i.e. all local rates of change are first calculated on a fixed-volume basis (analogous to an Eulerian treatment), and afterwards, dilatation effects are taken into account at the end of the time-step. The star marker * in the RHS of Eq. (22) indicates the Eulerian state after the time advancement ($\Delta y^* = \Delta y^n$).

Although it would also be possible to calculate open systems with the above mentioned procedure considering $\mathrm{d}P/\mathrm{d}t = 0$, we use instead the fully conservative approach suggested by Lignell et al. (2013) in this work.

References

Abdelsamie, A.; Lignell, D.; Thévenin, D.: Comparison Between ODT and DNS for Ignition Occurrence in Turbulent Premixed Jet Combustion: Safety-Relevant Applications. *Zeitschrift fuer Physikalische Chemie*, 231(10), (2017), 1709–1735.

Ashurst, W.; Kerstein, A.: One-dimensional turbulence: Variable-density formulation and application to mixing layers. *Physics of Fluids*, 17(2), (2005), 025107 1–27.

Cabra, R.; Chen, J.-Y.; Dibble, R. W.; Karpetis, A. N.; Barlow, R. S.: Lifted methane-air jet flames in a vitiated coflow. *Combustion and Flame*, 143(4), (2005), 491–506.

Echekki, T.; Kerstein, A.; Dreeben, T.: One-Dimensional Turbulence Simulation of Turbulent Jet Diffusion Flames: Model Formulation and Illustrative Applications. *Combustion and Flame*, 125(3), (2001), 1083–1105.

Fragner, M.; Schmidt, H.: Investigating asymptotic suction boundary layers using a one-dimensional stochastic turbulence model. *Journal of Turbulence*, 18(10), (2017), 899–928.

Goodwin, D.: *Cantera C++ User's Guide*. California Institute of Technology (2002).

Hindmarsh, A.; Serban, R.: *User Documentation for CVODE v2.8.2 (SUNDIALS v2.6.2)*. Lawrence Livermore National Laboratory (2015).

Jozefik, Z.; Kerstein, A.; Schmidt, H.; Lyra, S.; Kolla, H.; Chen, J.: One-dimensional turbulence modeling of a turbulent counterflow flame with comparison to DNS. *Combustion and Flame*, 162(8), (2015), 2999–3015.

Kerstein, A.: One-dimensional turbulence: model formulation and application to homogeneous turbulence, shear flows, and buoyant stratified flows. *Journal of Fluid Mechanics*, 392, (1999), 277–334.

Kerstein, A.; Ashurst, W.; Wunsch, S.; Nilsen, V.: One-dimensional turbulence: Vector formulation and application to free-shear flows. *Journal of Fluid Mechanics*, 447, (2001), 85–109.

Lignell, D.; Kerstein, A.; Sun, G.; Monson, E.: Mesh adaption for efficient multiscale implementation of One-Dimensional Turbulence. *Theoretical and Computational Fluid Dynamics*, 27(3), (2013), 273–295.

Lignell, D.; Lansinger, V.; Medina M., J. A.; Klein, M.; Kerstein, A.; Schmidt, H.; Fistler, M.; Oevermann, M.: One-dimensional turbulence modeling for cylindrical and spherical flows: model formulation and application . *Theoretical and Computational Fluid Dynamics*, 32(4), (2018), 495–520.

Lu, T.; Law, C.: A criterion based on computational singular perturbation for the identification of quasi steady state species: A reduced mechanism for methane oxidation with NO chemistry . *Combustion and Flame*, 154(4), (2008), 761–774.

Luong, M.; Yu, G.; Lu, T.; Chung, S.; Yoo, C. S.: Direct numerical simulations of ignition of a lean n-heptane/air mixture with temperature and composition inhomogeneities relevant to HCCI and SCCI combustion. *Combustion and Flame*, 162(12), (2015), 4566–4585.

Lyons, K.: Towards an understanding of the stabilization mechanisms of lifted turbulent jet flames: Experiments. *Progress in Energy and Combustion Science*, 33(2), (2007), 211–231.

Medina M., J. A.; Schmidt, H.; Mauss, F.; Jozefik, Z.: Constant volume n-Heptane autoignition using One-Dimensional Turbulence. *Combustion and Flame*, 190, (2018), 388–401.

Motheau, E.; Abraham, J.: A high-order numerical algorithm for DNS of low-Mach-number reactive flows with detailed chemistry and quasi-spectral accuracy. *Journal of Computational Physics*, 313, (2016), 430–454.

Oevermann, M.; Schmidt, H.; Kerstein, A.: Investigation of autoignition under thermal stratification using linear eddy modeling. *Combustion and Flame*, 155(3), (2008), 370–379.

Passot, T.; Pouquet, A.: Numerical simulation of compressible homogeneous flows in the turbulent regime. *Journal of Fluid Mechanics*, 181, (1987), 441–466.

Smith, G. P.; Golden, D. M.; Frenklach, M.; Moriarty, N. W.; Eiteneer, B.; Goldenberg, M.; Bowman, C. T.; Hanson, R. K.; Song, S.; Gardiner, W. C.; Lissianski, V. V.; Qin, Z.: *GRI-MECH 3.0*. `http://www.me.berkeley.edu/gri_mech/` (1999).

Yoo, C. S.; Lu, T.; Chen, J.; Law, C.: Direct numerical simulations of ignition of a lean n-heptane/air mixture with temperature inhomogeneities at constant volume: Parametric study. *Combustion and Flame*, 158(9), (2011), 1727–1741.

Yu, R.; Bai, X.: Direct numerical simulation of lean hydrogen/air auto-ignition in a constant volume enclosure. *Combustion and Flame*, 160(9), (2013), 1706–1716.

Address: Chair of Numerical Fluid Mechanics and Gas Dynamics, Faculty of Mechanical Engineering, Brandenburg University of Technology Cottbus-Senftenberg, Siemens-Halske-Ring 14, 03046 Cottbus, Germany
email: `Tommy.Starick@b-tu.de`